



Estimating $ZZ \rightarrow ll\nu\nu$ background in the $ll + E_T^{miss}$ final state using $Z\gamma \rightarrow ll\gamma$ data

A Thesis

submitted to

Indian Institute of Science Education and Research, Pune
in partial fulfillment of the requirements for the
BS-MS Dual Degree Programme

by

Mangesh Sonawane

Registration Number: 20121083



Indian Institute of Science Education and Research, Pune
Dr. Homi Bhabha Road,
Pashan, Pune 411008, INDIA

June 2017 - April 2018

Conducted at : DESY
Notkestraße 85,
22607, Hamburg
Germany

Supervisor: Dr. Beate Heinemann
©Mangesh Sonawane 2018
All rights reserved

Certificate

This is to certify that this dissertation, entitled "Estimating $ZZ \rightarrow ll\nu\nu$ background in the $ll + E_T^{miss}$ final status using $Z\gamma \rightarrow ll\gamma$ data", submitted towards the partial fulfilment of the BS-MS dual degree programme at the Indian Institute of Science Education and Research (IISER), Pune, represents the work carried out by Mangesh Sonawane at the Deutsches Elektronen-Synchrotron (DESY), Hamburg, under the supervision of Dr. Beate Heinemann, Professor of Experimental Particle Physics at the Institute of Physics, University of Freiburg, during the academic year 2017-2018.

Mangesh Sonawane

Dr. Beate Heinemann

Committee:

Dr. Beate Heinemann

Dr. Seema Sharma

I dedicate this thesis to my parents, Avinash and Ranjana Sonawane, my mentors, Dr. Sourabh Dube and Dr. Seema Sharma, and to my friends and colleagues and IISER, without whose timely advice and support this thesis would not have been made possible.

Declaration

I hereby declare that the matter contained within the thesis entitled "Estimating $ZZ \rightarrow ll\nu\nu$ background in the $ll + E_T^{miss}$ final state using $Z\gamma \rightarrow ll\gamma$ data", contains the results of the work carried out by me at the Deutsches Elektronen-Synchrotron (DESY) Hamburg, under the supervision of Dr. Beate Heinemann, and the same has not been submitted elsewhere for any other degree.

Mangesh Sonawane

Dr. Beate Heinemann

Committee:

Dr. Beate Heinemann

Dr. Seema Sharma

Acknowledgements

I would like to express my deepest gratitude for Dr. Beate Heinemann for her guidance and patient mentoring. It's not just technical skills that I have acquired under her supervision, but also an understanding of how a physicist approaches the subject and tackles the inevitable problems that surface.

⟨ placeholder ⟩

Abstract

In the search for Dark Matter (DM) at the LHC, SM particles are produced in association with DM particles, which are invisible as they don't interact with the detector. Thus events with large imbalance in transverse momentum are of interest. One such signature is $ll + E_T^{miss}$. The dominant background contributing to the search for DM in the $ll + E_T^{miss}$ is $ZZ \rightarrow ll\nu\nu$. Currently, this background is determined using Monte Carlo simulation, with an uncertainty of $\approx 10\%$ [2]. The goal of this study is to establish a data driven method to estimate this background, and reduce the uncertainty. Using $Z\gamma \rightarrow ll\gamma$, which is a process with low backgrounds and has a high $BR \times \sigma$, it is possible to estimate the $ZZ \rightarrow ll\nu\nu$ contribution. In regions where $p_T(\gamma) \gg M_Z$, the two processes are kinematically similar. They have the same production mechanisms, but differ due to the photon and Z boson couplings to the quarks being different, as well as the difference in mass (photons are massless, while Z bosons are massive). Introducing a transfer factor R as the ratio $\sigma(ZZ)/\sigma(Z\gamma)$ which is determined from simulation, the contribution of $ZZ \rightarrow ll\nu\nu$ to the background can be estimated from $Z\gamma \rightarrow ll\gamma$ data. The uncertainty on the prediction of R due to theoretical aspects is estimated in this work.

Contents

Abstract	i
1 Introduction	1
1.1 The Standard Model	2
1.2 Theoretical tools	4
1.2.1 Quantum Electrodynamics	4
1.2.2 Quantum Chromodynamics	4
2 The Large Hadron Collider	6
3 Analysis	8
3.1 Motivation	8
4 Theoretical uncertainties on cross sections and the transfer factor R	10
4.1 MCFM	11
4.2 Generator Parameters	11
4.3 Results	12
4.3.1 Uncertainty from Scale Variation	14
4.3.2 Uncertainty from PDF variation	15
4.3.3 Uncertainty from Photon Fragmentation	17

Chapter 1

Introduction

The Standard Model of physics is one of the most successful theories developed, describing the fundamental forces and their interactions. It is theoretically self-consistent, and has enjoyed tremendous success in providing stunningly accurate experimental predictions. However, the Standard Model is not complete theory. It does not provide an explanation for several observed phenomena, such as gravity, or the accelerating expansion of the universe, among others.

One such question that triggers burning curiosity is the apparent incongruity of galaxy rotation curves with the theory of Newtonian mechanics: stars in the arms of spiral galaxies appear to move much faster than Newtonian physics would predict. Either the current understanding of mechanics is incomplete, or there is more mass present somewhere in the galaxy that is not visible by any method that is currently employed. This invisible hunk of matter is what is termed as Dark Matter (DM).

Detailed observations of these rotation curves, along with measurements of other phenomena such as gravitational lensing by distant galaxies, galaxy clusters, and Cosmic Microwave Background (CMB) lead to the conclusion that, if the Dark Matter hypothesis is true, the amount of visible Baryonic matter in the universe is a mere 4%. The remaining 96% of the universe is composed of Dark Matter and Dark Energy.

Now it becomes important to address the question: what exactly is Dark Matter?

Several extensions to the Standard Model, called Beyond Standard Model (BSM) theories, attempt to provide an explanation of these observed phenomena. Dark Matter hasn't been observed to interact directly through the electromagnetic, strong or weak nuclear forces, consequently candidates for Dark Matter are called Weakly Interacting Massive Particles (WIMPs). In LHC experiments, events with WIMPs in the final state show up as an imbalance in the momentum in the plane transverse to the beam (referred to as E_T^{miss} throughout this thesis).

One such BSM theory postulates that these Dark Matter candidate particles may couple to Standard Model particles in interactions mediated by the Higgs boson. Fig 1.1 illustrates some of the possible processes for the production of the Higgs boson, where the Higgs boson further decays into invisible particles.



Figure 1.1: Feynman diagrams for the Standard Model production of the Higgs boson; VH: Higgs produced in association with a W/Z boson (top left), ggF: gluon-gluon fusion (top right), VBF: vector boson fusion (bottom left), ttH: (bottom right). The Higgs boson then further decays into invisible DM particles.

In this thesis, a closer look is taken at the VH channel, in particular ZH , where the Higgs boson decays invisibly into DM particles, and the Z boson decays into a dilepton pair. The signature of such a process is $ll + E_T^{miss}$. A Dark Matter search in this channel would be to stack all known Standard Model processes that contribute to the $ll + E_T^{miss}$ signal (these form the background) and look for excesses which will indicate the presence of non Standard Model processes. In this thesis, a closer look is taken at the $ZZ \rightarrow ll\nu\nu$ process, which constitutes the dominant SM background in the $ll + E_T^{miss}$ final state. However, it is difficult to discriminate between the Standard Model $ZZ \rightarrow ll\nu\nu$ and $ZH \rightarrow l^+l^- + E_T^{miss}$, the process under consideration, because of the identical final state. Thus, an attempt is made to estimate it using alternate processes with clean signals.

1.1 The Standard Model

The Standard Model is the name given to the theory of particles, fundamental forces, and interactions that govern the Universe. It describes three of the four forces: the electromagnetic, strong and weak forces. Figure 1.2 shows a schematic representation of the elementary particles in the Standard Model.

The Standard Model classifies fundamental particles as either Fermions or Bosons:

- **Fermions:** make up the matter in the universe. Fermions are spin 1/2 particles, and are subdivided into two categories, quarks and leptons. Quarks exist in 6 flavors, up, down, charmed, strange, top (or truth) and bottom (or beauty). Leptons too are in 6 flavors: electrons, muons, and taus, and their respective neutrinos. The up, charmed and top quarks carry a charge of $+2/3e$. The down, strange and bottom quarks carry a charge of $-1/3e$. The electron, muon and tau carry a charge of $-1e$, and the neutrinos are chargeless. Here, e is the unit of electronic charge, and is equal to $1.602e^{-19}$ Coulombs. Quarks and leptons are divided into three generations, with each generation having more mass than the last. Each fermion has a parity inverted counterpart, called an anti-particle, having the same mass, but an opposite charge. For example, an anti-electron (or a positron) has a charge of $+1e$ and a down anti-quark will have charge of $+1/3e$.
- **Bosons:** are particles with integral spin that mediate the interactions between particles in the universe. There are four gauge bosons: the photon, which mediates electromagnetic interactions, the W and Z bosons that mediate weak interactions, and the gluons, which mediate strong interactions. These are vector bosons, having spin $+1$. In addition, there is a scalar boson (spin 0), the Higgs boson, which gives particles their mass.

Standard Model of Elementary Particles

three generations of matter (fermions)				
	I	II	III	
mass	$\approx 2.4 \text{ MeV}/c^2$	$\approx 1.275 \text{ GeV}/c^2$	$\approx 172.44 \text{ GeV}/c^2$	0
charge	$2/3$	$2/3$	$2/3$	0
spin	$1/2$	$1/2$	$1/2$	0
QUARKS	u up	c charm	t top	g gluon
	d down	s strange	b bottom	γ photon
	e electron	μ muon	τ tau	Z Z boson
LEPTONS	ν_e electron neutrino	ν_μ muon neutrino	ν_τ tau neutrino	W W boson
	$< 2.2 \text{ eV}/c^2$	$< 1.7 \text{ MeV}/c^2$	$< 15.5 \text{ MeV}/c^2$	$\approx 80.39 \text{ GeV}/c^2$
	0	0	0	± 1
	$1/2$	$1/2$	$1/2$	1
				SCALAR BOSONS
				GAUGE BOSONS

Figure 1.2: A schematic representation of the Standard Model of particles. The table shows the three generations of fermions (classified as quarks and leptons) that are the building blocks of all known matter in the universe, and bosons that mediate interactions, and are thus responsible for 'forces'

The Standard Model addresses three of the four fundamental forces; it does not address the Gravitational force. These interactions can be described by the $SU(3) \times SU(2) \times U(1)$ local gauge symmetry group, where the $SU(3)$ symmetry group describes the strong interaction, and the electroweak interactions are based on the $SU(2) \times U(1)$ symmetry group. There are $8+3+1$ generators associated with this model, each generator corresponding to a vector boson.

Thus, there are 8 gluons, which are massless spin 1 particles with an intrinsic property called color charge, that mediate strong interactions (described by Quantum Chromodynamics). They are responsible for interactions between quarks (leptons do not interact via the strong force) as they have a non vanishing color charge. At low energies, quarks cannot be found in isolation, instead occurring in triplets called *Baryons*, or a bound quark-antiquark pair, called *Mesons*. This is because of color confinement.

The interaction of the scalar Higgs field with the vector fields W^+ , W^- , W^0 and B causes the spontaneous breaking of the $SU(2) \times U(1)$ symmetry, resulting in 3 massive and one massless gauge boson. It also implies the existence of a neutral scalar boson, known as the Higgs boson, which was discovered in July 2012[1]. The generators of $SU(2) \times U(1)$ correspond to the W^+ , W^- and Z bosons, massive vector bosons (spin 1) that mediate weak interactions, and the massless vector boson γ (photon), which mediates electromagnetic interactions. The W bosons are charged, whereas the Z boson and γ are neutral.

The Standard Model is based on the formalism of quantum field theories, in which particles are interpreted as excitations of underlying fields.

1.2 Theoretical tools

1.2.1 Quantum Electrodynamics

Quantum Electrodynamics (QED) is the relativistic quantum field theory of electromagnetism. It encompasses all particles having a charge (which includes all the quarks and charged leptons, and their charged composite particles), and the photon as the mediator of interactions between these.

Quantum Electrodynamics is extended to describe the electroweak theory, which includes neutrinos, and the W and Z bosons as mediators of interactions.

1.2.2 Quantum Chromodynamics

Quantum Chromodynamics (QCD) is the quantum field theory of strong interactions. It describes particles that have color charge (such as quarks, and their composite particles), and is mediated by gluons.

QCD has some interesting properties. For example, the force between two color charges remains constant, the force between two quarks increases with the separation, a phenomenon known as asymptotic freedom. Thus, to separate them, increasing amounts of energy must be put in, leading to

Chapter 2

The Large Hadron Collider

Chapter 3

Analysis

3.1 Motivation

Chapter 4

Theoretical uncertainties on cross sections and the transfer factor R

It is worth reiterating that the goal of this thesis is to use $Z\gamma \rightarrow ll\gamma$ process to estimate the dominant contribution $ZZ \rightarrow ll\nu\nu$ to the Standard Model $ll + E_T^{miss}$ background. Excesses would indicate the presence of BSM physics. It is thus important to have an estimate of the uncertainties on the theoretical predictions of the ZZ and $Z\gamma$ cross sections, and the transfer factor R .

In this study, the following sources of uncertainties are studied.

- **Scale Uncertainties:** contributions due to higher order QCD corrections cannot be calculated to arbitrarily high order, as it gets progressively more computationally expensive. Thus, this study is limited to Next to Leading Order (NLO), and further corrections are accounted for as scale uncertainties.
- **PDF Uncertainties:** a proton-proton collision involves the interaction of the composite quarks and gluons (partons) at very high energies. These partons carry a fraction of the proton momentum. Parton Distribution Functions (PDFs) represent this fraction of proton momentum carried by partons as probability distributions. Owing to the non-deterministic nature of this fact, this study attempts to account for this uncertainties as PDF uncertainties.
- **Photon Fragmentation Uncertainties:** in the $Z\gamma \rightarrow ll\gamma$ process, the signal includes a photon. However, while reconstructing the event, soft photons, or photons resulting from other fragmentation processes may be encountered. To ensure that the photon is indeed prompt, it is required to be isolated from hadronic activity (such as pion decays). This isolation is implemented experimentally in different ways. The uncertainty associated with the implementation of this isolation is estimated as photon fragmentation uncertainties.

To characterize these uncertainties, we use a programme, MCFM, to generate cross sections for $ZZ \rightarrow ll\nu\nu$ and $Z\gamma \rightarrow ll\gamma$ processes, and vary the relevant parameters such as scale, PDF sets, and photon isolation effects to obtain an estimate of the uncertainties.

4.1 MCFM

MCFM is a program that calculates cross sections for femtobarn-level processes at LO or NLO. In this study, MCFM v8.0 [5] is used to produce cross sections of $ZZ \rightarrow ll\nu\nu$ and $Z\gamma \rightarrow ll\gamma$ processes at NLO, with a selection of generator level cuts. The generation parameters in MCFM allow fine control over the sample, such as PDF sets, photon isolation, lepton and photon p_T and η , renormalization and factorization scales, etc. The samples are generated with cuts on $E_T^{miss} = p_T(Z \rightarrow \nu\nu)$ for the ZZ process and $p_T(\gamma)$ for the $Z + \gamma$ process. A ratio of these cross sections is taken to obtain the R distribution as a function of p_T . The uncertainty on R is calculated by varying several parameters at the generator level, such as the renormalization and factorization scales, the PDF sets used, photon fragmentation, etc. The contributions of the $q\bar{q}$ and gg processes are estimated separately.

In MCFM generated events containing a leptonically decaying Z boson, $Z \rightarrow ee$ only i.e. the decay is constrained to just one flavor, electrons. As electrons and muons have similar properties with the exception of mass, simply the branching fraction of $Z \rightarrow ee$ must be accounted for to obtain the inclusive value of R .

$$R_{inc} = R * \frac{BR(Z \rightarrow ee)}{BR(Z \rightarrow ee) * BR(Z \rightarrow \nu\nu) * 2} \quad (4.1)$$

4.2 Generator Parameters

The samples are generated using MCFM v8.0 for the following data points:

$$\begin{aligned} \text{For } ZZ \rightarrow ee\nu\nu : E_T^{miss} &> \{50, 75, 100, 125, 150, 200, 250, 300, 400, 500\} \text{ GeV} \\ \text{For } Z(\rightarrow ee) + \gamma : p_T(\gamma) &> \{50, 75, 100, 125, 150, 200, 250, 300, 400, 500\} \text{ GeV} \end{aligned} \quad (4.2)$$

Table 4.1 lists the generator level settings used for the ZZ and $Z + \gamma$ processes. All lepton cuts are consistent with the ones used in the ATLAS $Z + E_T^{miss}$ analysis.

Cuts	$ZZ \rightarrow ee\nu\nu$	$Z(\rightarrow ee) + \gamma$
Process ID	87	300
M_{ee}	$81 < M_{ee} < 101 \text{ GeV}$	$81 < M_{ee} < 101 \text{ GeV}$
$M_{\nu\nu}$	-	-
Order	NLO	NLO
PDF set	CT14	CT14
$p_T^{\text{lead}}(e)$	$> 30 \text{ GeV}$	$> 30 \text{ GeV}$
$ \eta^{\text{lead}}(e) $	< 2.47	< 2.47
$p_T^{\text{sublead}}(e)$	$> 20 \text{ GeV}$	$> 20 \text{ GeV}$
$ \eta^{\text{sublead}}(e) $	< 2.47	< 2.47
Renormalization scale	$91.187 \text{ GeV } (M_Z)$	$91.187 \text{ GeV } (M_Z)$
Factorization scale	$91.187 \text{ GeV } (M_Z)$	$91.187 \text{ GeV } (M_Z)$

Table 4.1: Settings in input.DAT for MCFM

The constraint on M_{ee} in the case of $Z + \gamma$ suppresses the FSR process by ensuring that the lepton pair are from a Z decay only.

4.3 Results

Using the settings listed in Table 4.1, the cross sections for $ZZ \rightarrow ee\nu\nu$ and $Z\gamma \rightarrow ee\gamma$ are generated, as shown in Figure 4.1. Throughout this analysis, these samples are the reference.

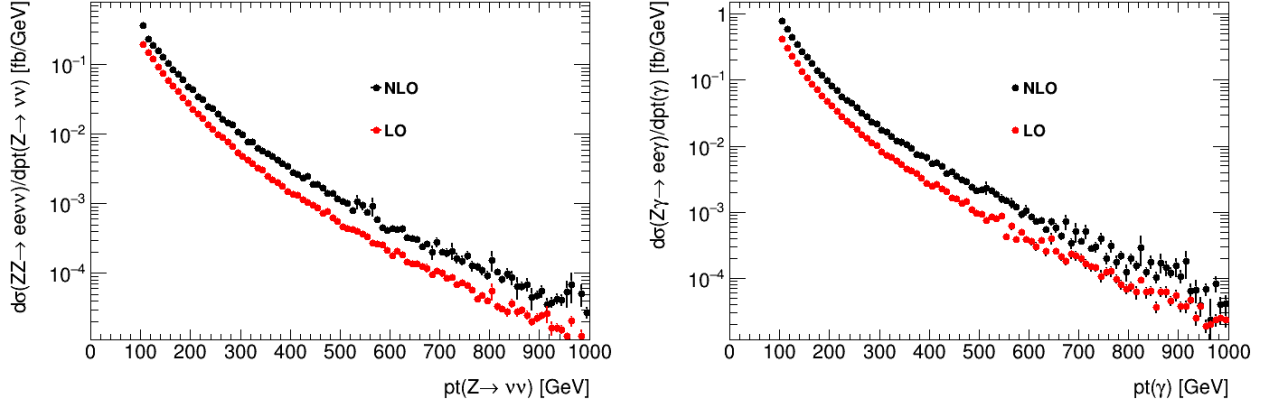


Figure 4.1: NLO and LO cross sections of $ZZ \rightarrow ee\nu\nu$ (left) and $Z\gamma \rightarrow ee\gamma$ (right) processes with the cuts as in Table 1. The vertical axis is in \log_{10} scale. The leptonically decaying Z boson decays to an e^+e^- pair. There is no flavor constraint on the neutrinos.

The ratio $R = \sigma(ZZ \rightarrow ee\nu\nu)/\sigma(Z\gamma \rightarrow ee\gamma)$ is shown in Figure 4.2, where 10 samples for each process are generated, following the prescription in Equation 4.2.

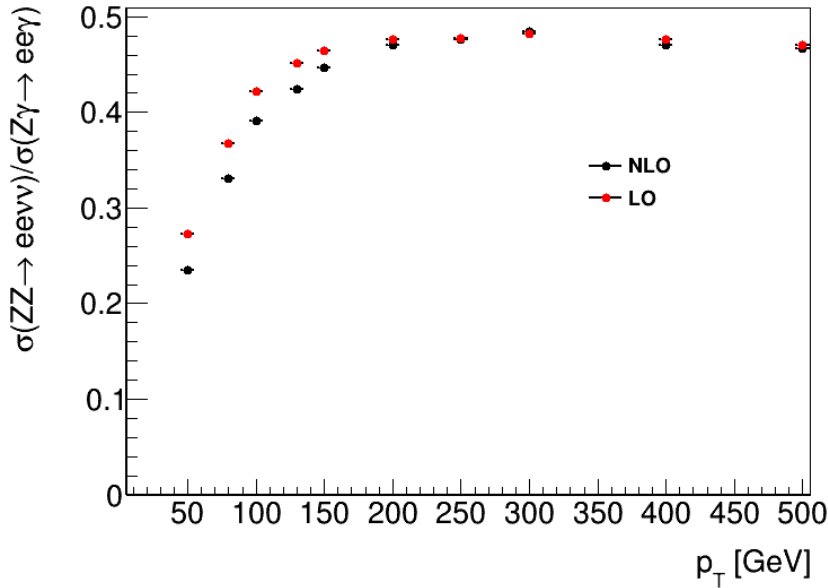


Figure 4.2: The transfer factor R as a function of p_T , taken as a ratio of the $ZZ \rightarrow ee\nu\nu$ and $Z\gamma \rightarrow ee\gamma$ cross sections at both LO and NLO. The leptonically decaying Z boson decays to an e^+e^- pair.

The R value is observed to increase from ≈ 0.24 at 50 GeV to ≈ 0.47 at high p_T , where it is constant. When the branching ratio of Z boson decaying selectively to e^+e^- , or to $\nu\nu$, is accounted for as shown in Equation 4.1, the resulting ratio $R(p_T)$ is shown in Figure 4.3, which shows the ratio of $\sigma(ZZ)$ to $\sigma(Z\gamma)$, i.e. if the Z bosons do not decay further. The value of R is observed to increase from ≈ 0.61 at 50 GeV to ≈ 1.2 at high p_T , in reasonable agreement with the simple approximate calculation presented in Section 2 of $R \approx 1.28$.

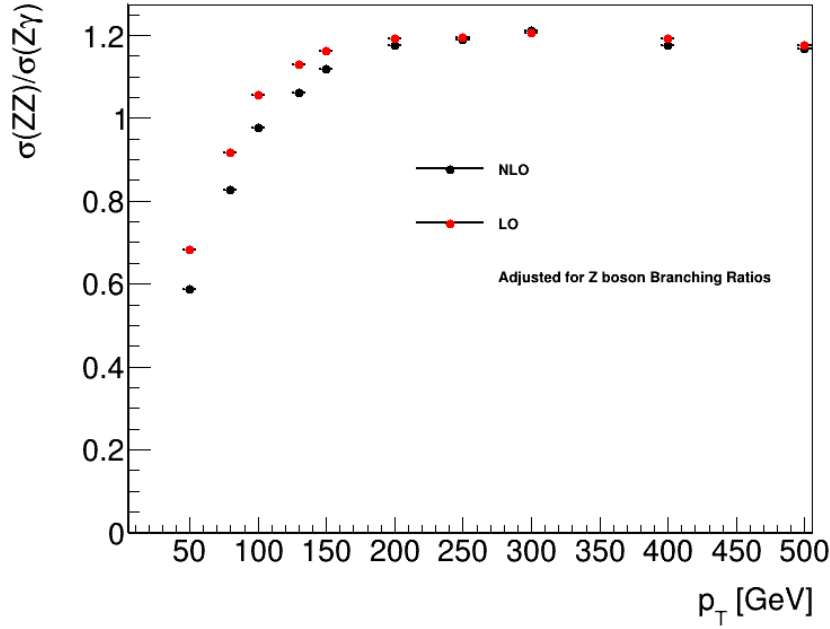


Figure 4.3: The transfer factor R as a function of p_T at both LO and NLO, adjusted for the $Z \rightarrow ee$ and $Z \rightarrow \nu\nu$ branching ratios. This shows the $R = \sigma(ZZ)/\sigma(Z\gamma)$, where the Z bosons do not decay.

Gluon-gluon processes contribute to 8.6% of the total cross section for the ZZ process and 2.5% of the $Z + \gamma$ process. Figure 4.4 shows the ZZ and $Z\gamma$ cross sections (Z boson decay constrained to only e^-e^+ and $\nu\bar{\nu}$ only) from the contributing $q\bar{q}$, qg and gg subprocesses.

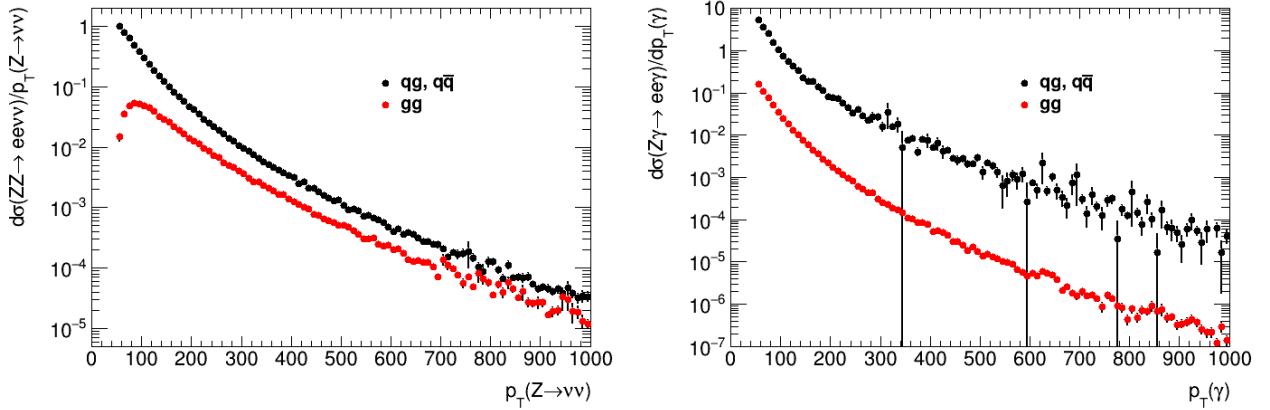


Figure 4.4: The cross sections of $ZZ \rightarrow ee\nu\nu$ (left) and $Z\gamma \rightarrow ee\gamma$ (right) as a function of p_T , from the contributing $q\bar{q}$, qg and gg processes. The leptonically decaying Z boson decays to an electron-positron pair

The R_{gg} distribution, shown in Figure 4.5 is observed to approach an asymptotic value at a much higher $p_T = 1.5$ TeV. The shape and scale of the R_{gg} distribution remain to be understood, as they differ from Figure 4.2.

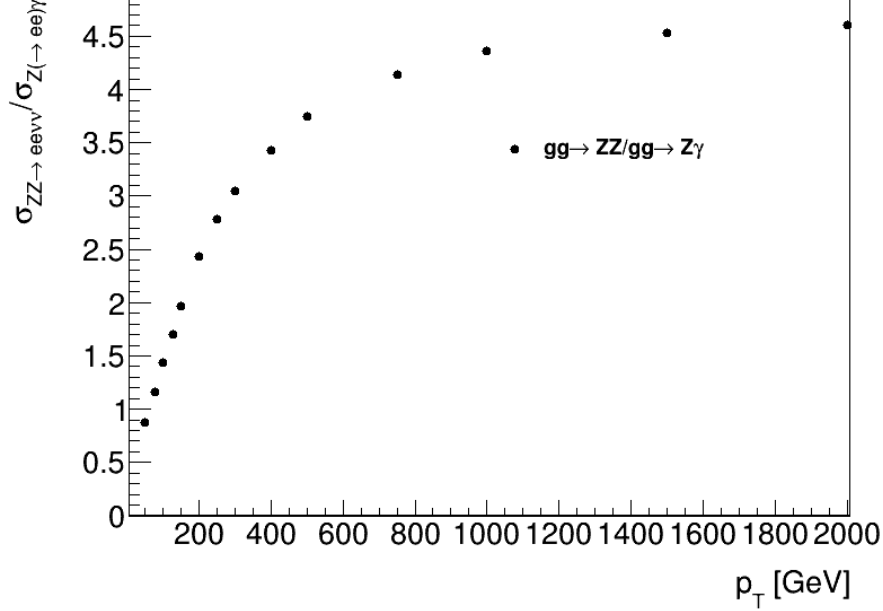


Figure 4.5: $R_{gg}(p_T)$, computed from the contributions of the gg subprocess to the cross sections of ZZ and $Z\gamma$. The curve reaches a plateau at a much higher p_T than for contributions from the $q\bar{q}$ process only.

4.3.1 Uncertainty from Scale Variation

In higher order QCD calculations, perturbative corrections may be added to the vertices or propagators in a Feynman diagram. Physically, these corrections occur at very small time scales. These loop integrals that correspond to these corrections diverge.

The higher the order, the more difficult the calculation is. It is possible to introduce an arbitrary cut-off scale μ such that up to a given order, the effect of these corrections can be absorbed into the strong coupling constant $\alpha_s(\mu)$.

Two kinds of divergences are encountered: infrared divergences, and ultraviolet divergences. Infrared divergences occur for an on-shell internal propagator, and ultraviolet divergences are logarithmic divergences that occur as the integration variable approaches ∞ . They correspond to physics at long and short distances¹, respectively. The infrared divergences are addressed by the inclusion of the factorization scale μ_F , while the ultraviolet divergences are addressed by the inclusion of the renormalization scale μ_R . These parameters are arbitrary, and are set by hand. These are then varied between $\frac{1}{2}\mu < \mu < 2\mu$ to obtain an indication of the dependence of the matrix element on the scales, and thus, the uncertainty around the chosen scale.

To address scale uncertainties in this study, the prescription used in Ref [6], section 4 is followed. The central scale, μ_0 is chosen to be $H_T/2$ for both $ZZ \rightarrow ll\nu\nu$ and $Z\gamma \rightarrow ll\gamma$ samples (where H_T is the scalar sum of the transverse momentum of all particles after collision, $\sum_i p_{T,i}$), and seven-point variations are applied, i.e.

$$\frac{\mu_i}{\mu_0} = (1, 1), (1, 2), (2, 1), (2, 2), (0.5, 1), (1, 0.5), (0.5, 0.5) \quad (4.3)$$

where $i = 0, \dots, 6$. The central cross section value is taken to be the mean of the maximum and minimum cross sections resulting from this variation, and the uncertainty to be the half the difference

¹Long distances are those where soft interactions take place, away from the hard parton-parton interaction. Short distances are those where the hard parton-parton interactions occur.

between the same.

$$\sigma_{NLO}^{(V)} = \frac{1}{2} \left[\sigma_{NLO}^{(V,max)} + \sigma_{NLO}^{(V,min)} \right] \quad (4.4)$$

$$\delta\sigma_{NLO}^{(V)} = \frac{1}{2} \left[\sigma_{NLO}^{(V,max)} - \sigma_{NLO}^{(V,min)} \right] \quad (4.5)$$

where

$$\begin{aligned} \sigma_{NLO}^{(V,max)} &= \max \left\{ \sigma_{NLO}^{(V)}(p_T(V), \mu_i) | 0 \leq i \leq 6 \right\} \\ \sigma_{NLO}^{(V,min)} &= \min \left\{ \sigma_{NLO}^{(V)}(p_T(V), \mu_i) | 0 \leq i \leq 6 \right\} \end{aligned} \quad (4.6)$$

and $V = Z \rightarrow \nu\nu$ for $ZZ \rightarrow ll\nu\nu$, or $V = \gamma$ for $Z\gamma \rightarrow ll\gamma$. This uncertainty is propagated to R .

To estimate the degree of correlation between the processes, the process dependent part of the cross sections may be used. Since the study is conducted at NLO, the highest available term in the perturbative expansion is considered to define a K-factor.

$$\Delta K_{NLO}^{(V)} = \sigma_{NLO}^{(V)}(p_T) / \sigma_{LO}^{(V)}(p_T) \quad (4.7)$$

To estimate the unknown process dependent correlation effects, the difference between the QCD K-factors of the $ZZ \rightarrow ll\nu\nu$ and $Z\gamma \rightarrow ll\gamma$ processes is taken.

$$\delta^{(2)}\sigma_{NLO} = \Delta K_{NLO}^{(\gamma)}(p_T) - K_{NLO}^{(Z)}(p_T) \quad (4.8)$$

4.3.2 Uncertainty from PDF variation

A proton is a Baryon, i.e. it is composed of 3 quarks and several gluons. In a proton-proton collision, it is these quarks and gluons, called *partons* that actually interact. This is illustrated by Figures *the feynman diagrams in Chapter 3*, which show the Feynman diagrams for quark-quark and gluon-gluon interactions. Thus it is important to know the momentum of the interacting partons. It is not possible to deterministically know the momentum of the partons, as it is the momentum of the protons that is set during the experiment. However, the fraction of the proton momentum that is carried by the partons can be modelled as probability distributions.

Parton Distribution Functions (PDFs) characterize the fraction of proton momentum carried by partons as probability distributions. PDF sets are collections of PDFs that model the uncertainty associated with parton momenta. The PDF set used for reference is the CT14[7] PDF set. The uncertainty on the PDFs is studied by using the 30 variations provided by the PDF4LHC15 set[8], constructed from the combination of CT14, MMHT14[9] and NNPDF3.0[10] PDF sets. These sets are provided by LHAPDF6[11]. PDF4LHC15 provides a set of variations that include those determined by different groups (MSTW, CTEQ and NNPDF). The set used here is PDF4LHC15_nlo_30, consisting of 30 members. While the most accurate uncertainties are given by PDF4LHC15_nlo_100 set, PDF4LHC15_nlo_30 is used here for a faster, reasonably accurate estimate of the uncertainties.

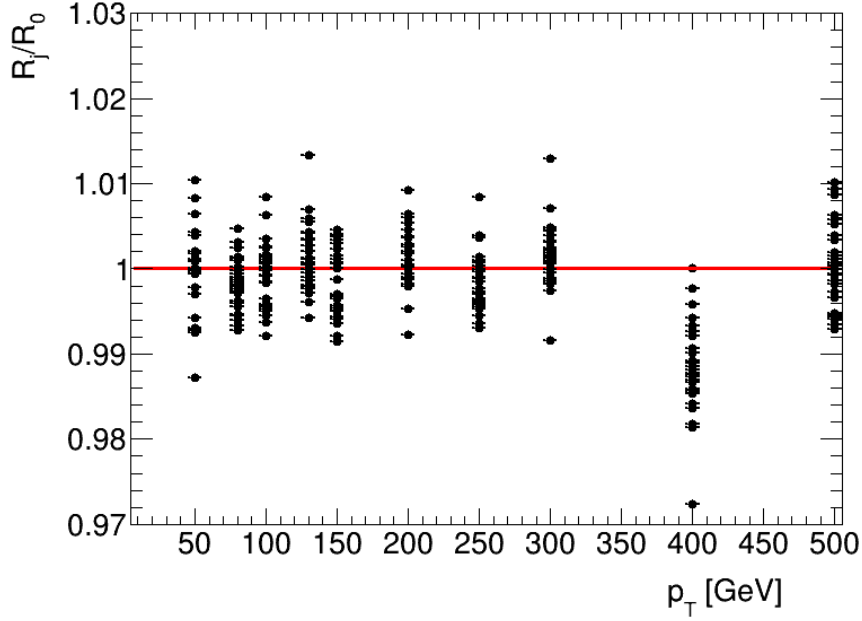


Figure 4.6: The relative ratio R_i/R_0 , of the transfer factor $R = \sigma(ZZ)/\sigma(Z\gamma)$ calculated using PDF sets 1-30, with respect to set 0 which is taken as the central value.

Fig.4.6 shows the comparison of the ratio $R(p_T)$ from the 30 member sets of PDF4LHC15_nlo_30. To measure the uncertainty due to these 30 sets, analogous to Equation 20 in Ref [8], Equation 4.9 is used:

$$\delta^{PDF} R = \sqrt{\sum_{k=1}^{N_{mem}} (R^{(k)} - R^{(0)})^2} \quad (4.9)$$

where N_{mem} is the number of member sets in the group, in this case, 30. The R distribution obtained from the PDF4LHC15_nlo_30 set is compared to the reference distributions from CT14, as shown in Figure 4.7:

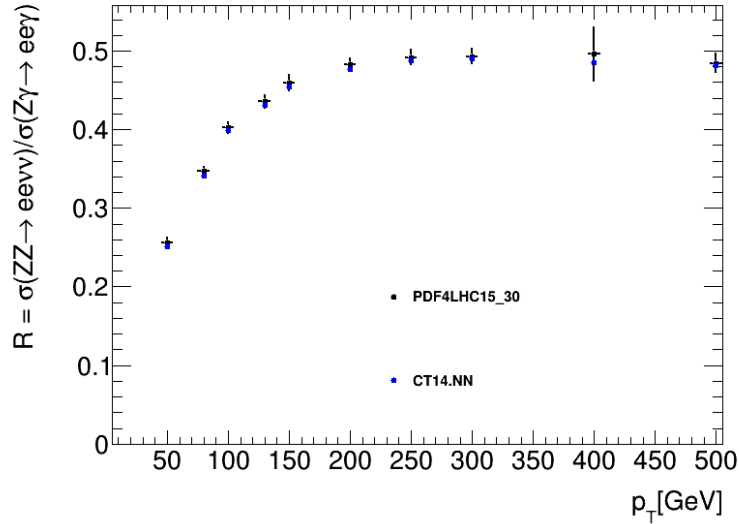


Figure 4.7: The ratio $R(p_T)$ calculated using the PDF sets in PDF4LHC15_nlo_30 with combined uncertainties as given by Equation 4.9 (blue), compared to the reference constructed from the PDF set CT14 (red).

Figure 4.7 shows a comparison between the central value of the sets in PDF4LHC15_nlo_30 with the

combined uncertainties, and the reference PDF set CT14. The combined uncertainty around $R \approx 0.40$ is $\pm 2.00\%$ at 100 GeV. The R distributions drawn from the two PDF sets agree to within the uncertainty bounds.

4.3.3 Uncertainty from Photon Fragmentation

The $Z\gamma \rightarrow ll\gamma$ process may contain photons that arise from the hadron showers. It is therefore important to isolate the prompt photon from hadronic activity. This reduces unwanted background from pion decays, or fragmentation processes.

Experimentally, photon isolation is implemented with the following cuts:

$$\sum_{\in R_0} E_T(\text{had}) < \epsilon_h p_T^\gamma \quad \text{or} \quad \sum_{\in R_0} E_T(\text{had}) < E_T^{\text{max}} \quad (4.10)$$

limiting the transverse hadronic energy $E_T(\text{had})$ in a cone of size $R_0 = \sqrt{\Delta\eta^2 + \Delta\phi^2}$ around the photon, to some fraction of the photon p_T , or some fixed small cut-off.

The smooth cone isolation method of Frixione [12] is an alternative isolation procedure, which simplifies calculations by avoiding fragmentation contributions. The following isolation prescription is applied to the photon:

$$\sum_{R_{j\gamma} \in R_0} E_T(\text{had}) < \epsilon_h p_T^\gamma \left(\frac{1 - \cos R_{j\gamma}}{1 - \cos R_0} \right)^n. \quad (4.11)$$

where $R_{j\gamma}$ is the separation of the photon and the j^{th} hadron. This requirement constrains the sum of hadronic energy inside a cone of radius $R_{j\gamma}$, for all separations $R_{j\gamma}$ less than a chosen cone size R_0 . This prescription allows soft radiation inside the photon cone, but collinear singularities are removed. The smooth cone isolation is infrared finite, thus fragmentation contributions do not need to be included.

The relative isolation, given by Equation 4.3.3 is used in experimental analyses, while smooth isolation is difficult to implement experimentally. However, comparing both methods gives us an estimate of the uncertainty due to the modelling of photon fragmentation.

In this analysis, R_0 is chosen to be 0.4 to agree with the experimental definition. The central value is chosen to be from the sample using smooth cone isolation (Frixione) with $\epsilon_h = 0.075$ and $n = 1$. These parameters are varied within a reasonable range to assess the uncertainty as shown in Figure 4.8.

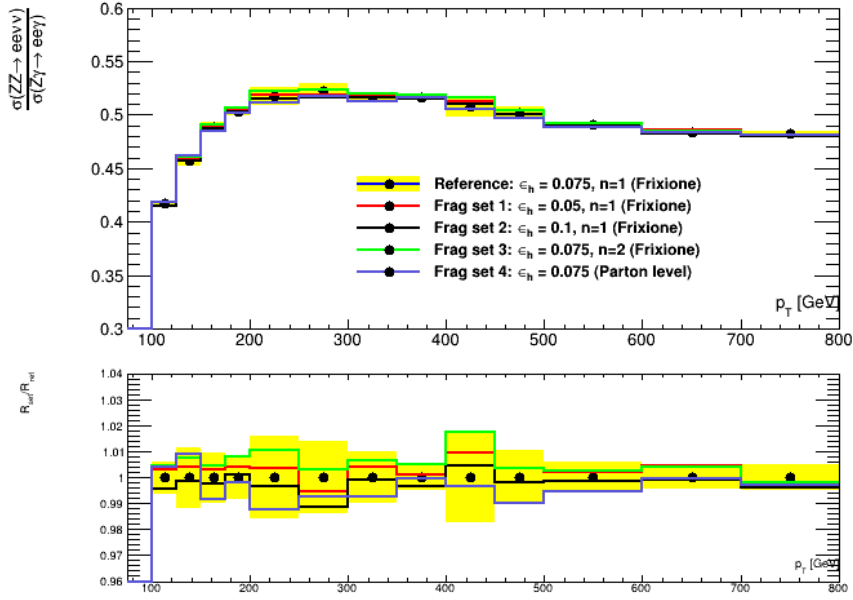


Figure 4.8: R distribution as a function of p_T , showing the uncertainty due to variation of photon isolation parameters ϵ_h and n in the smooth cone isolation procedure (Frixione), and ϵ_h in the photon isolation procedure. The lower panel shows the relative deviation of the varied sets from the central value, as well as the uncertainty band.

The uncertainty is calculated from the four sets listed in Figure 4.8:

$$\begin{aligned} \delta R_i &= |R_i - R_{ref}| & i \in (1, 2, 3, 4) \\ \delta R &= \sqrt{\max_{i=1,2,3} (\delta R_i)^2 + (\delta R_4)^2} \end{aligned} \quad (4.12)$$

as the effects assessed by changing the isolation definition in set 4, and varying the parameters in sets 1-3 are different.

The uncertainty is $< 2\%$ over the whole range, which has been extended up till 800 GeV.

Bibliography

- [1] *Observation of a New Particle in the Search for the Standard Model Higgs Boson with the ATLAS Detector at the LHC*
ATLAS Collaboration
arXiv:1207.7214
- [2] *Search for an invisibly decaying Higgs boson or dark matter candidates produced in association with a Z boson in pp collisions at $\sqrt{s} = 13$ TeV with the ATLAS detector*
ATLAS Collaboration
arXiv:1708.09624
- [3] *Using γ + jets to calibrate the Standard Model $Z(\rightarrow \nu\nu)$ + jets background to new processes at the LHC*
S. Ask, M. A. Parker, T. Sandoval, M. E. Shea, W. J. Stirling
Cavendish Laboratory, University of Cambridge, CB3 0HE, UK; 2011
[arXiv:1107.2803]
- [4] *2017 Review of Particle Physics - Particle Listings*
C. Patrignani et al. (Particle Data Group)
Chin. Phys. C, 40, 100001 (2016)
- [5] *Monte Carlo for FeMtobarn processes (MCFM) v8.0 User Manual*
John Campbell, Keith Ellis, Walter Giele, Ciaran Williams
<https://mcfm.fnal.gov/>
- [6] *Precise predictions for V+jets dark matter backgrounds*
J.M. Lindert, S. Pozzorini, et al.
arXiv:1705.04664
- [7] *New parton distribution functions from a global analysis of quantum chromodynamics*
Sayipjamal Dulat, Tie Jiun Hou, Jun Gao, Marco Guzzi, Joey Huston, P. Nadolsky, Jon Pumplin, Carl Schmidt, Daniel Stump, C. P. Yuan
arXiv:1506.07443
- [8] *PDF4LHC recommendations for LHC Run II*
[arXiv:1510.03865]
- [9] *Parton distributions in the LHC era: MMHT 2014 PDFs*
L. A. Harland-Lang, A. D. Martin, P. Motylinski, R. S. Thorne
arXiv:1412.3989
- [10] *Parton distributions for the LHC Run II*
The NNPDF Collaboration: Richard D. Ball, Valerio Bertone, Stefano Carrazza, Christopher S. Deans, Luigi Del Debbio, Stefano Forte, Alberto Guffanti, Nathan P. Hartland, Jose I. Latorre, Juan Rojo, Maria Ubiali
arXiv:1410.8849

- [11] *LHAPDF6: parton density access in the LHC precision era*
Andy Buckley, James Ferrando, Stephen Lloyd, Karl Nordstrom, Ben Page, Martin Ruefenacht, Marek Schoenherr, Graeme Watt
arXiv:1412.7420
- [12] *Isolated photons in perturbative QCD*
S. Frixione
Phys. Lett.B429(1998)369–374, hep-ph/9801442